Impact of Near-Angle Scatter on Exo-Earth Coronagraphy

H. Philip Stahl, David D. Smith, and Bijan Nemati

NASA MARSHALL SPACE FLIGHT CENTER, HUNTSVILLE, AL 35812

ABSTRACT

Near-Angle Scatter (NAS) of the host star's light may limit the ability of a potential Habitable Worlds Observatory (HWO) to detect and characterize an Earth-like planet around a Sun-like star via coronagraphy. NAS from each optical surface produces an E-field across the dark hole that is coherent. These E-fields sum and could be as large or larger than the coronagraph mask leakage E-field. NAS E-fields contribute to the dark hole noise floor via both shot noise and heterodyne amplification of the wavefront instability. The amount of NAS is determined entirely by the statistical properties of the optical surface microroughness and the operating wavelength. Surface properties include not only the rms roughness, but also correlation length and the functional form of the distribution itself. This paper derives an expression that specifies the surface statistics required to achieve a given coronagraph error budget NAS throughput allocation. Analysis does not include scatter from coating columnar structure, edges, contamination, micrometeoroid impacts, or polarization.

Keywords: near angle scatter, space telescopes, coronagraphy

1.0 INTRODUCTION

Near Angle Scatter (NAS) may limit the ability of a potential Habitable Worlds Observatory (HWO) to detect and characterize a potential exo-Earth located 50 to 100 milli-arc-seconds (mas) from its host star via coronagraphy. In 2023, we published a first-order single-surface analysis that derived 'placeholder' specifications for the primary mirror using Rayleigh-Rice Vector Scatter Theory, Generalized Harvey-Shack Scalar Scatter Theory, and Greynolds Approximation. **[1]** For an arbitrary 1E-11 throughput error budget allocation, the primary mirror specification was: Static Surface Roughness < 1 nm rms, and Dynamic Surface Roughness < 1 pm PV. These specifications are consistent with other analyses. **[2-3]** The 2023 paper did not include scatter from other surfaces, primary mirror segment edges, coating structure, contamination, micrometeoroid impacts, etc.

Near-Angle Scatter (NAS) of the host star's light from each optical surface produces an E-field across the dark hole that is coherent. These NAS E-fields sum – they do not RSS – and could be as large or larger than the coronagraph mask leakage E-field. These NAS E-fields contribute to the dark hole noise floor via both shot noise and heterodyne amplification of the wavefront instability. The E-field amplitude is determined entirely by the statistical properties of the optical surface microroughness and the operating wavelength. Surface properties include not only the rms roughness, but also correlation length and the functional form of the distribution itself.

This paper derives an expression that specifies the surface statistics required to achieve a given coronagraph error budget NAS throughput allocation. Our analysis is purely analytical and does not include the effects of surface contamination, diffraction, or scatter from segment edges, coating columnar structure, or polarization.

2.0 SCIENCE REQUIREMENT DRIVES SPECIFICATIONS

Direct imaging of exoplanets requires coronagraph/telescope systems capable of rejecting the light from the host star and enabling imaging of its companions. The potential Habitable Worlds Observatory (HWO) desires to detect and characterize Earth-like planets in the habitable zone of nearby sun-like stars. Viewed from a distance of 10 pc, such planets would have an angular separation of 100 mas (0.1″) at maximum separation. (Fig 1) The flux ratio of the planet's reflected light at quadrature phase relative to its host star's direct light can be estimated to be 2.1×10^{-10}, or 210 ppt (parts-per-trillion). **[2]**

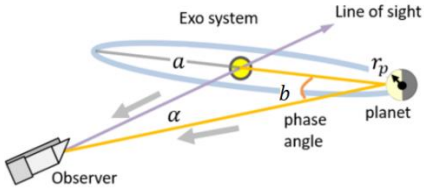

Fig. 1 The flux ratio of an exoplanet depends on its radius, orbital semi-major axis, and the phase angle.

Coronagraphs (Fig 2) achieve this flux ratio by blocking the star's light with a focal plane mask (FPM). The planet's light, which comes in at a slight angle, misses this mask and proceeds. After recollimation, a 'Lyot' mask removes most (but

not all) of the remaining on-axis light. The beam is then focused onto the image plane of a detector, creating what is usually referred to as a 'dark hole,' a zone where host star light has been strongly suppressed. The key attributes of any coronagraph needed to derive a direct-imaging error budget are core throughput, inner and outer working angles, and raw contrast. [2] For the purpose of our Near-Angle Scatter study, the key parameter is contrast.

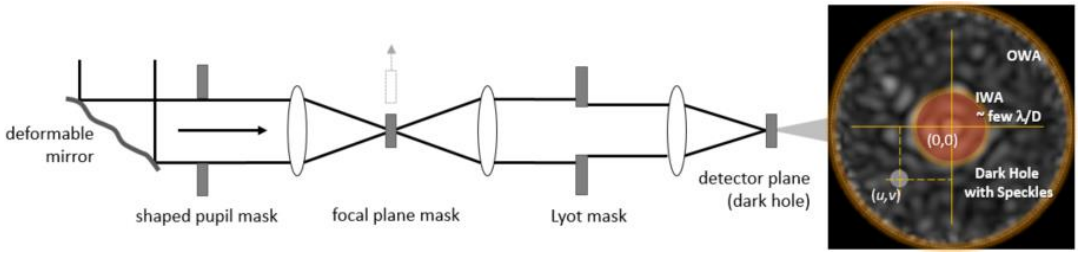

Fig. 2 Typical coronagraph setup. Incoming light from the left is shaped in phase by a deformable mirror (or in phase and amplitude by two separated deformable mirrors), then sent through a succession of masks. The result in the final focal plane is a 'dark hole' where (on-axis) starlight is strongly suppressed relative to the (off-axis) planet light. The inner and outer working angles (IWA, OWA, respectively, denote the limits of the coronagraph suppression region (the "dark hole").

For a 210 ppt exo-Earth target, to be observed with SNR = 7, the total error from all sources combined must be less than 30 ppt. Fig. 3 plots the total random noise and its constituents as a function of integration time. Also plotted in Fig 3 is the maximum allowable systematic error from residual speckle, i.e. the quadrature difference between the total allowable error (30 ppt) and the total random error. For an integration time of 25 hours, the total expected random error is about 15.6 ppt and the total allowed residual speckle error is about 25.6 ppt.

As discussed in Nemati et. al. [2], this error allocation flows down to a raw contrast error budget allocation of 4×10^{-11}. For this analysis, we assume a 10^{-11} NAS allocation error budget.

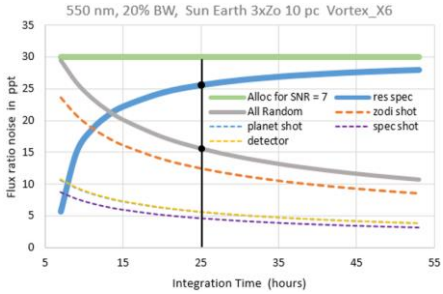

Fig. 3 Relative contributions to the flux ratio noise from the main noise sources versus integration time. (Planet shot noise trace is beneath detector trace.)

2.1 Contrast

Contrast is the measure of the effectiveness of the coronagraph in suppressing starlight near the planet and is defined as the ratio of two throughputs.

$$C(u,v) \equiv \frac{\tau\,(u,v)}{\tau_{pk}\,(u,v)},$$

where $\tau_{pk}(u,v)$ is the "peak" throughput or fraction of the star's light, if it were located at (u,v), detected within a solid angle region of interest Ω_r centered at (u,v) relative to the total light incident upon the primary mirror. And, $\tau(u,v)$ is throughput, which is defined as the ratio of power at position (u,v) divided by total incident power from the star, in its nominal position of $(0,0)$.

$$\tau(u,v) \equiv \frac{\Phi\,(u,v)}{\Phi_i\,(0,0)},$$

If a coronagraph were perfect, then $\tau(u,v)$ would be zero. But coronagraphs are not perfect. Typically, the only sources of noise considered for throughput are leakage around the coronagraph mask due to design inefficiency and leakage due to wavefront instability. This analysis identifies a third leakage source, near-angle scatter. There could also be other sources.

$$\tau(u,v) = \tau_{(Coronagraph\ Leakage)} + \tau_{(Wavefront\ Instability)} + \tau_{NAS} + \ldots$$

2.2 Heterodyne Amplification

At the end of the wavefront control procedure that gives the coronagraph its final level of starlight suppression, some residual optical error remains, leading to a 'leakage' field $E(u,v)$ in the image plane. This leakage E-field produces a speckle intensity pattern given by $|E(u,v)|^2$. When a disturbance or drift error occurs in the opto-mechanical configuration

of the telescope or coronagraph, the E-field changes by a small amount – coherently adding a perturbation field $\Delta E(u, v, t)$ to the 'initial' or 'static' part of the field $E(u, v)$. The coherent mixing of the original field E and perturbation field ΔE creates a speckle pattern, the intensity of which is given by:

$$|E + \Delta E|^2 = |E|^2 + |\Delta E|^2 + 2\,\mathcal{R}\{E^* \cdot \Delta E\}\,.$$

It is this mixed or heterodyned term for which error budgets allocate a maximum value. Typical error budgets assume that the static E-field is entirely caused by coronagraph mask inefficiency when deriving a wavefront instability specification. But near-angle scatter can increase the static E-field. And consequently, to keep the heterodyne term constant, the wavefront instability must become smaller. Also, if NAS increases the static E-field, then it also increases its shot noise.

3.0 SCATTERED LIGHT

For an ideal telescope/coronagraph system (one with a perfect wavefront, i.e. no aberrations, and no scatter), the telescope produces an ideal point spread function (PSF) of the host star and the coronagraph blocks its light completely, allowing light from the exo-Earth to be detected and characterized. But, even in a perfect system, diffraction produces some leakage. And, in an imperfect system, wavefront or amplitude errors (whose distribution in spatial frequency can be described by their power spectral density – PSD) can scatter light out of the host star's PSF and onto the exo-Earth's PSF (Fig 4). PSD is typically divided into 3 spatial frequency regimes: Low, Mid and High. The low-spatial frequency regime (dominated by figure errors) determines the shape of the PSF core. Mid-spatial frequency errors produce small-angle scatter which broaden the PSF. High-spatial frequency micro-roughness produces wide angle and uniform Lambertian scatter across the entire PSF.

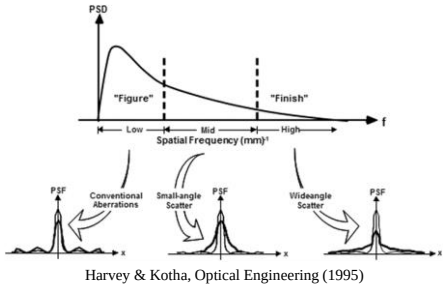

Harvey & Kotha, Optical Engineering (1995)

Fig 4: Surface (or wavefront) spatial frequency error scatters light out of core PSF. **[4]**

Surface structure (low, mid, and high) that can be decomposed into specific spatial frequencies scatters (actually diffracts) light out of the PSF to specific angles. We refer to these spatial frequencies as 'correlated' surface structure. Our 2023 paper presented processes for deriving 'placeholder' specifications for the primary mirror using Rayleigh-Rice Vector Scatter Theory, Generalized Harvey-Shack Scalar Scatter Theory, and Greynolds Approximation. For an arbitrary 10^{-11} throughput error budget allocation, the primary mirror specification was: Static Surface Roughness < 1 nm rms, and Dynamic Surface Roughness < 1 pm PV. **[1]**

Surface structure that cannot be decomposed into specific spatial frequencies diffusely scatters light into all angles. We refer to this as 'uncorrelated' surface structure. An example of an uncorrelated scattering is a Lambertian surface which scatters incident light uniformly into all projected solid angles. Again, this type of scatter is also called diffuse.

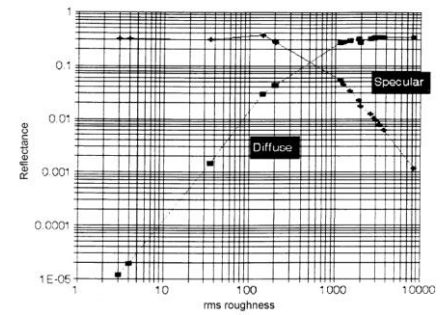

Fig 5: Conservation of Energy balances Specular and Diffuse Scatter. **[5]**

First key point: by conservation of energy, assuming no transmission or absorption, all light incident upon a surface comes off of that surface via one of three mechanisms: specular reflection, correlated scatter/diffraction or uncorrelated/diffuse scatter. The amplitude of each component of this reflection depends upon the surface's roughness. (Fig 5) The smoother the surface, the smaller the amplitude of its diffuse scatter. But all surfaces, even super polished surfaces, have some amount of uncorrelated microstructure and thus have some amount of diffuse scatter.

Because the host star is in the field of view, every optical surface is a scattering source with a direct path to the detector. Host star light directly illuminates the primary mirror. The primary mirror scatters some of that irradiance into an angle which, after reflecting off the secondary mirror spreads energy across the coronagraph dark hole, including in the region of the exo-Earth signal. Next, some the host star light (specular reflection of PM) incident on the secondary mirror is scattered across the PSF and into the dark hole. And so on for the tertiary and quaternary mirrors. At this point it is very important to note that scattered light sums. (Fig 6) It does not root-sum-square (RSS) like wavefront errors.

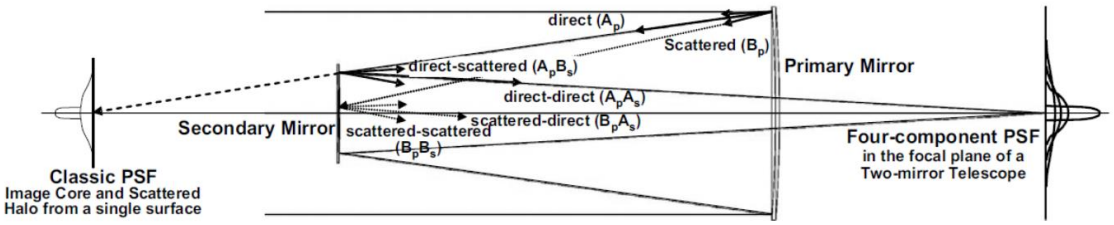

Fig. 6 Each surface in telescope/coronagraph optical train is an 'in-field' source of near-angle scatter which sums in focal plane. **[6]**

It is also important to note that the scattered E-fields are constructively coherent with the leakage E-field. Because the scattered light is from the host star light, there is no phase difference. Because the optical surfaces are very smooth (nanometers rms), the optical path difference is much smaller than the host star light's coherence length (micrometers) – because the coronagraph spectral band is narrow (i.e. < 20%).

Finally, scattered E-fields from the primary mirror are collimated in the dark hole. Consider a single point scatter on the primary mirror. The secondary and aft optics reimage that scattering source into a conjugate plane in the coronagraph. In Fig 2, the pupil mask is located at this plane. And, per Fig 2, a diverging point source in the pupil mask plane is collimated focused and recollimated into the dark hole. Now consider that the primary mirror's uncorrelated microstructure can be decomposed into billions or trillions of point scatterers each contributing a very small constructively coherent collimated E-field into the dark hole. Similarly, the secondary mirror contributes E-fields, which, while not collimated, have radii on the order of 30 meters.

3.1 Surface Power Spectral Density (PSD) and Auto-Covariance Function (ACF)

PSD decomposes any data set into contributions per frequency (spatial or temporal). The PSD of a data set can be calculated two ways: either by taking the modulus square of the Fourier transform of the data set, or by taking the Fourier transform of the autocovariance function (ACF) of the data set. (Fig 7) The ACF of a data set is calculated by taking its autoconvolution, i.e., shearing the data set against itself.

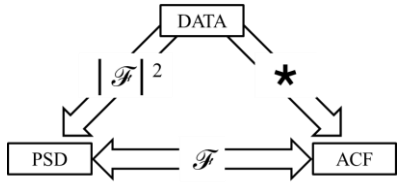

Fig. 7 PSD is modulus square of data set Fourier transform or Fourier transform of data set's autocovariance function.

Because PSD has been used to describe statistics of data as diverse as lithographic linewidths, surfaces (optical, roads, fields, oceans, etc.) to flow rates in the Nile River (Hurst exponent), its mathematical form and representation is well understood. A typical PSD is described by three parameters: PSD(0) (zero-frequency value of PSD); correlation length, ℓ; and the roughness exponent H (for Hurst). (Fig 8) **[7]**

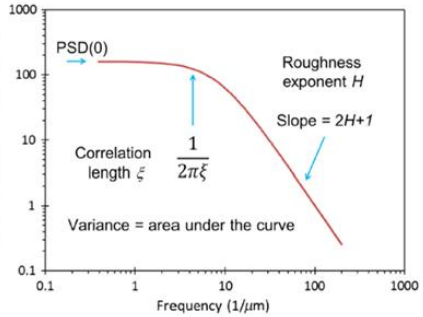

Fig. 8 Graphical representation of PSD. **[7]**

For optical surfaces, the PSD to the 'right' of the correlation length cutoff falls off as a statistical function with negative slope. For polished surfaces this slope is typically between -2 and -3. This region of the PSD describes the surface's structure that can be decomposed into correlated spatial frequencies – spatial frequencies which scatter light into discrete angles via the grating equation. The PSD to the 'left' of the correlation length cutoff is flat because at these spatial frequencies surface structure is uncorrelated. Thus, they scatter diffusely into these angles. (Fig 9) As a reminder, the PSD of an ideal Lambertian surface is simply a flat line for all spatial frequencies. Obviously, correlation length is important.

3.2 Correlation Length

Correlation Length (ℓ) is the maximum shear for which the surface spatial structure is correlated (i.e., the longest spatial wavelength Fourier decomposed periodic component). Surface structure separated by a distance larger than the correlation length are statistically independent, i.e., uncorrelated. Some define ℓ to be where the ACF equals zero, others define it as where the ACF equals 1/e. It is important to understand that the correlation length calculated from a data set is 'band limited'. If the surface is smooth, then it is either L or L/2 where L = sample length (depending on how correlation length is defined).

3.3 Band limited Data

The problem with calculating PSD (and ACF) from measured surface data is that no single instrument can cover the entire frequency range. Measured data is band-limited, therefore, calculations of PSD (and ACF) are band-limited. (Fig. 9) The longest spatial period (lowest spatial frequency) is limited by sample length. The shortest spatial period (highest spatial frequency) is limited by pixel size and Nyquist spacing. Interferometers and micro-profilometers can measure from one cycle across their data set (maybe half cycle) to a few hundred cycles. Interferometers typically measure a surface's full aperture. While micro-profilers (and sub-aperture interferometers) sample the surface. Micro-profilers measure areas of a few millimeters. Each instrument provides a band-limited measured RMS roughness estimate:

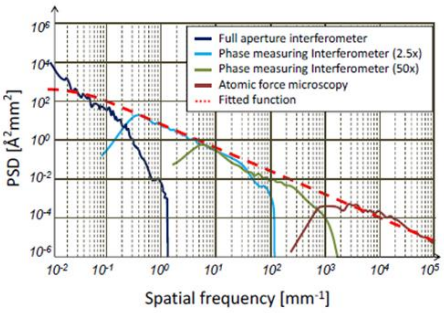

Fig. 9 Measured PSD is band-limited. **[8]**

$$\sigma = \left[\int_{f_1}^{f_2} PSD(f)df\right]^{1/2}$$

Total RMS roughness for the surface is obtained by RSS'ing the band-limited estimates: $\sigma^2_{Total} = \sigma^2_{Low} + \sigma^2_{Mid} + \sigma^2_{High}$

While it is well known that instruments are band-limited in their measurement of surface statistics, what is less well known is how these band-limited estimates impact near angle scatter. The answer requires a somewhat complicated but linear development. First, if PSD is band-limited, then so is ACF. The total ACF of a surface is the summation of individual band limited ACFs. Each instrument produces its own ACF with its own band-limited estimate of RMS roughness and correlation length. (Fig 10) It is important to understand that the correlation length of a given measurement may be due to the instrument's limitation and not the surface statistics. For example, the low and mid-spatial frequency correlation length due to the instrument's band limits and not the surface.

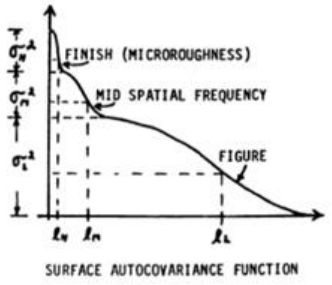

Fig. 10 Measured PSD is band limited. **[9]**

Next, a surface's total PSD (or PSF) is a stack of their band-limited estimates. (Fig 11 & 12) The reason is because no single instrument can measure the scattered light caused by surface structure outside of its band limits.

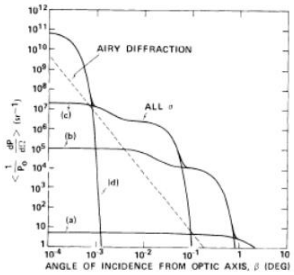

Fig. 11 Angle Resolved Scatter (ARS) vs angle of incidence. Dotted line is Airy Diffraction envelope. Solid lines are scattered light. **[10]**

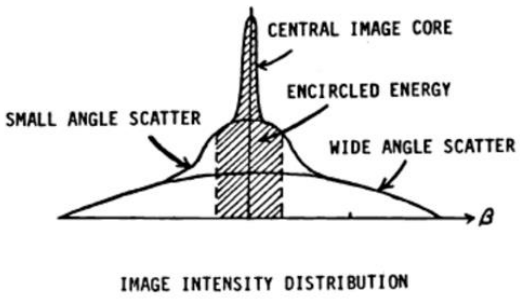

Fig. 12 Point Spread Function (PSF) is sum (stack) of diffraction and scatter. **[9]**

And again, it is important to emphasize that an instrument's 'measured' correlation length estimate may be artificial, the surface's true correlation length may be outside of the instrument's band-limit measurement range. It is interesting to note in Fig 11 that the correlation length cut-off for the low and mid-spatial estimates occurs at the diffraction limit – which implies that it is a measurement limit. While the micro-roughness cut-off is beyond the diffraction limit – implying that it is the true correlation length of the surface. Applying this observation to Fig 9 one might speculate that that surface's true correlation length is approximately 10 micrometers. This speculation is consistent with the fact that that surface was a super-polished EUV mirror. **[8]**

Second Key Point: So, what does this mean for near-angle scatter? The answer is: even if one removes all a mirror's correlated low- and mid-spatial frequency surface structure, either via computer-controlled polishing or a deformable mirror, the surface will always have some amount of microstructure. While the spatially correlated portion of this microstructure scatters (diffracts) light into large angles, the spatially uncorrelated portion of this microstructure diffusely scatters light into all angles, including angles very close to the specular reflection. (see Figs 13 and 14)

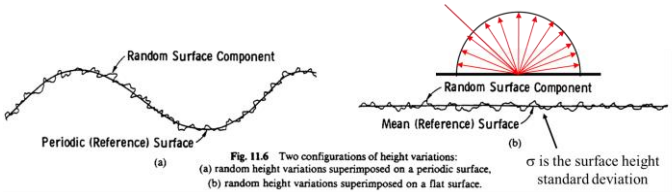

Fig. 11.6 Two configurations of height variations: (a) random height variations superimposed on a periodic surface, (b) random height variations superimposed on a flat surface.

Fig. 13 All surfaces consist of correlated and uncorrelated structure. Microstructure remains after removing low-frequency structure. **[11]**

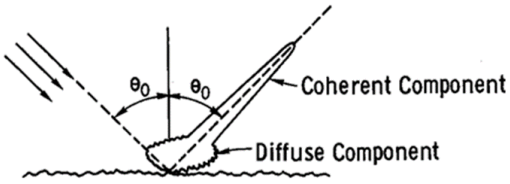

Fig. 14 Scatter consists of large coherent component and small diffuse component. **[11]**

3.4 Importance of Correlation Length and Distribution Functional Form

While typically overlooked, Correlation Length (ℓ) may be the most important parameter for Near-Angle Scatter. According to Beckmann-Kirchhoff theory **[5]**, for an isotropic random surface with normal (Gaussian) height distribution much smaller than the illuminating wavelength and a Gaussian autocorrelation function, the PSD is determined by a surface's microstructure rms roughness, σ, and correlation length, ℓ,

$$\mathrm{PSD}_{2D}(f) = \pi\, \ell^2\, \sigma^2\, e^{-(\pi \ell f)^2},$$

where f is spatial frequency. Thus, the amplitude of the near-angle 'Lambertian' scatter is given by $\mathrm{PSD}_{2D}(0) = \pi\, \ell^2\, \sigma^2$.

Fig 15 shows that for two surfaces with the same RMS roughness, the surface with the longer correlation length (i.e. the smoother surface) has a higher $\mathrm{PSD}_{1D}(0)$. Thus, this surface will have higher near-angle scatter.

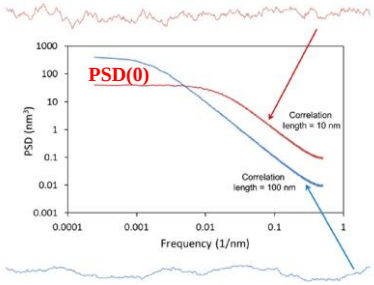

Fig. 15 $\mathrm{PSD}_{1D}(0)$ depends on roughness and correlation length. **[7]**

More generally, PSD is often represented by an inverse power law model,

$$PSD_{2D}(f) = \frac{KAB}{[1 + (Bf)^2]^{(C+1)/2}},$$

where:

$$PSD_{2D}(0) = KAB = \frac{C-1}{2\pi}(B\sigma)^2 \quad \text{if C > 1 [12].}$$

In the case of $C = 2$, the PSD profile is Lorentzian. Thus, from the inverse Fourier transform, the ACV is a decaying exponential, and B is the 1/e correlation length. In the case where $C = 2\pi^2 + 1$, the equation for $PSD_{2D}(0)$ profile is Gaussian and $B = \ell$. Going forward, we will consider the Gaussian and Lorentzian cases as representative of the upper and lower bounds on $PSD_{2D}(0)$ and, therefore, on the NAS, respectively. Note that the Gaussian case has a $PSD_{2D}(0)$ that is a factor $(2\pi^2 + 1)/2$ greater than the Lorentzian case, given the same values of B and σ.

3.5 Bidirectional Reflectance Distribution Function (BRDF)

BRDF (defined by Nicodemus in 1977 **[13]**) is a geometric relationship to describe surface scatter in radiometric terms. (Fig 16) BRDF is a defined as the reflected radiance, L, (power per unit solid angle per unit projected area) divide by the incident irradiance, E, (power per unit area). **[5, 14]** (Please note that the international standard (SI) radiometric irradiance E notation is different from electric field E vector.)

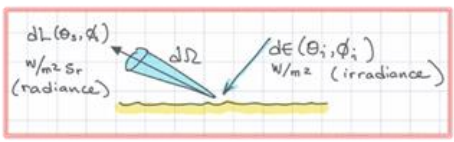

Fig 16: BRDF Defining Geometry

$$BRDF\ (\theta_s,\ \varphi_s;\ \theta_i,\ \varphi_i) = \frac{dL\ (\theta_s,\ \varphi_s;\ \theta_i,\ \varphi_i)}{dE\ (\theta_s,\ \varphi_s;\ \theta_i,\ \varphi_i)} = \frac{\Phi_s/\Omega}{\Phi_i cos\ (\theta_s, \varphi_s)} = \frac{\Phi_s/\Omega}{\Phi_i}$$

where:

Φ_i	= Total Power Incident on Entrance Pupil, i.e. Primary Mirror Area, = $E_i \; x \; A_{PM}$
Φ_s/Ω	= Power per unit Solid Angle Scattered from Entrance Pupil, i.e. PM Area
$(\theta_s, \varphi_s; \theta_i, \varphi_i)$	= (Nλ/D, Nλ/D; 0, 0) where N = 1 to 30 so that (θ_s, φ_s) are very small

BRDF is frequently plotted in $(\beta - \beta_0)$ space where $\beta = \sin(\theta_s)$, $\beta_0 = \sin(\theta_i)$.

Thus, the scattered power from the PM, directly imaged into a dark hole pixel is given by:

$$\Phi_s(u,v)_{Core} = \text{BRDF}(\lambda/D < (\beta - \beta_0) < N\lambda/D) \;\cdot\; \Phi_i \;\cdot\; \Omega_{Core}$$

3.6 BRDF and PSD

Rayleigh-Rice (RR) theory relates the PSD of an isotropic (i.e. polished) surface to BRDF **[5]**:

$$\text{PSD}(f_x, f_y) = \left[\frac{10^8 \lambda^4}{16\pi^2}\right] \cdot \text{BRDF}(\beta - \beta_0) \; [\text{Å}^2 \; \mu m^2]$$

For small angles, the equation simplifies to PSD_0 and $BRDF_0$, because both are constant across the dark hole.

$$\text{PSD}_0 = \left[\frac{10^8 \lambda^4}{16\pi^2}\right] \cdot \text{BRDF}_0 \; [\text{Å}^2 \; \mu m^2]$$

4.0 DERIVING SURFACE SPECIFICATION FOR NEAR-ANGLE SCATTER

Using the definition for Throughput (Sec 2.1) and BRDF (Sec 3.5), we now define **Near-Angle Scatter Throughput** as the ratio of power scattered off an optical surface (e.g. primary mirror) and imaged into the dark hole relative to the power incident on optical surface.

$$\text{NAS Throughput} = \tau_{NAS} = \frac{\Phi_{NAS}(u,v)}{\Phi_i} = BRDF\,(2\lambda/D) \;\cdot\; \Omega_{Core}$$

$$BRDF_0 = \frac{\tau_{NAS}}{\Omega_{Core}}$$

Now, using the relationship between BRDF and PSD (Sec 3.6); and the relationship between PSD and surface statistics (Sec 3.4), a general expression can be derived that specifies an optical surface's statistics to meet a given near-angle scatter throughput error budget allocation:

$$\sigma \, \ell < \frac{\lambda^2}{4\pi} \sqrt{\left(\frac{2\pi}{C-1}\right) \frac{\tau_{NAS}}{\Omega_{core}}}.$$

Thus, given an allocation for τ_{NAS}, the maximum permissible values for σ and ℓ for a particular functional form (corresponding to C) can be determined. For a Gaussian PSD the previous equation becomes:

$$\sigma\ell < \frac{\lambda^2}{4\pi} \sqrt{\frac{\tau_{NAS}}{\pi \Omega_{core}}}.$$

As discussed above, BRDF, surface PSD, and NAS throughput are all proportional to one another. Fig. 17(a) plots these quantities for scattering angles and surface spatial frequencies across the dark hole for three different values of rms roughness (10, 1 and 0.1 nm rms), assuming a correlation length of $\ell = 100\mu m$. For each roughness value a colored band is shown, the band's width represents the effect of the PSD's functional form, i.e., Gaussian at the top to Lorentzian at the bottom. Note that NAS is independent of angle within the dark hole. Thus, Fig. 17(b) plots the NAS vs. roughness at a single angle within the dark hole, for three discrete values of the correlation length (10, 100 and 1000 μm). Note the NAS increases quadratically with both σ and ℓ, as expected from the equations for $PSD_{2D}(0)$ above. In this case, each band corresponds to a different correlation length. This figure encapsulates the importance of these statistics (σ and ℓ) as well as the functional form of the PSD itself to meeting the throughput specification. For example, if the primary mirror was specified to have a τ_{NAS} allocation of 10^{-12}, it would need to have $\sigma < 3$Å to ensure the entire band of C values at

$\ell = 100\mu m$ is within the specification. But, if the mirror is super-polished such that its $\ell = 10\mu m$ (i.e., remove spatial period surface structure with periods > 10 μm), then the surface only needs to have $\sigma < 30$Å to meet its specification.

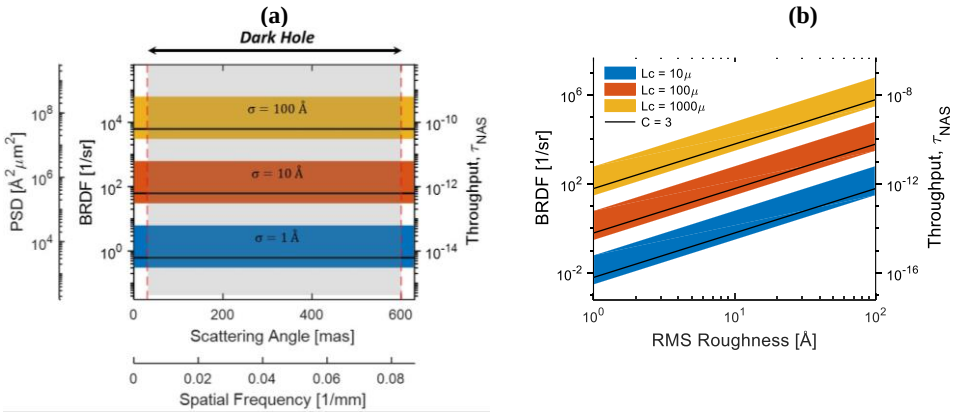

Fig 17: (a) BRDF, PSD, and core throughput vs. scattering angle and spatial frequency for three different values of RMS roughness and correlation length = 100 μm. (b) BRDF and NAS Core Throughput vs. RMS Roughness for three different values of correlation length. Band widths represent effect of PSD functional form, ranging from Gaussian ($C = 2\pi^2 + 1$) at top to Lorentzian ($C = 2$) at bottom. The black lines are for $C = 3$. The wavelength is 300 nm (shortest coronagraph wavelength) and the core solid angle was $\Omega_{core} = 10^{-14} sr$. The dashed red vertical lines in (a) represent the extent of a typical dark hole.

Using Gaussian statistics as the upper bound limit ensures that the entire band meets the throughput requirement. For λ and ℓ in μm, and roughness in Å

$$\sigma[\text{Å}] < \frac{\lambda^2 \cdot 10^4}{4\pi\ell}\left[\frac{\tau_{NAS}}{\pi\Omega_{core}}\right]^{1/2},$$

where $\Omega_{core} = \pi\theta_{core}^2/4 = \pi(\lambda/D)^2/4 \sim 0.01$ pico − Steradians. Per Sec 2.0, we assume a τ_{NAS} allocation of 10^{-11}.

But as discussed in Sec 3.0, this allocation needs to be distributed across all the surfaces before the coronagraph focal plane mask. Thus, for the purpose of this analysis, we allocated $\tau_{NAS} = 10^{-12}$ to each surface. Table 1 gives the maximum microroughness specification for each surface as determined from the above equation as a function of wavelength.

Table 1: Surface RMS Microstructure [Å] to have NAS Throughput < 1E-12				
	Wavelength (λ) [μm]			
Correlation Length (ℓ) [μm]	0.300	0.680	1.000	1.800
10	180.0	924.8	2000.0	6480.0
100	18.0	92.5	200.0	648.0
1000	1.8	9.2	20.0	64.8
10000	0.2	0.9	2.0	6.5

Obviously, the shortest coronagraph science wavelength drives the surface specification. And correlation length is important. But there is another key performance metric, RMS slope **[15]**, as shown in Table 2, which may be more intuitive, i.e., it provides an angular spread of a specular beam.

$$RMS\ Slope = \sqrt{2}\frac{\sigma}{\ell}$$

Table 2: Surface RMS Slope [μrad] to have NAS Throughput < 1E-12				
	Wavelength (λ) [μm]			
Correlation Length (ℓ) [μm]	0.300	0.680	1.000	1.800
10	572.8	2942.7	6364.0	20619.2
100	5.7	29.4	63.6	206.2
1000	0.1	0.3	0.6	2.1
10000	0.0	0.0	0.0	0.0

5.0 CONCLUSIONS

Near Angle Scatter (NAS) of the host star's light off of optical surfaces such as the primary mirror may limit the ability of a potential Habitable Worlds Observatory to detect and characterize a potential Earth-like planet around a Sun-like star via coronagraphy. NAS from each optical surface before the coronagraph focal plane mask produces an E-field across the dark hole that is coherent. These E-fields sum and could be as large or larger than the coronagraph mask leakage E-field. NAS E-fields contribute to the dark hole noise floor via both shot noise and heterodyne amplification of the wavefront instability. The amount of NAS is determined entirely by the statistical properties of the optical surface microroughness and the operating wavelength. Surface properties include not only the rms roughness, but also correlation length and the functional form of the distribution itself. Alternatively, the surface microstructure can be defined via a slope specification. We have derived an expression that specifies the surface statistics required to achieve a given coronagraph error budget NAS throughput allocation. This analysis does not include scatter from coating columnar structure, edges, contamination, micrometeoroid impacts, or polarization.

REFERENCES

1. H. Philip Stahl, "Assessment of near-angle scatter on exo-Earth coronagraphy," Proc. SPIE 12676, (4 October 2023); https://doi.org/10.1117/12.2676543
2. Nemati, Bijan, H. Philip Stahl, Mark T. Stahl, Garreth J. Ruane, Leah J. Sheldon, "Method for deriving optical telescope performance specifications for Earth-detecting coronagraphs," J. Astron. Telesc. Instrum. Syst. 6(3), 039002 (2020), doi: 10.1117/1.JATIS.6.3.039002.
3. Laurent Pueyo, Roser Juanola-Parramon, Jason Tumlinson, Rémi Soummer, Iva Laginja, Heidi B. Hammel, C. Mattias Mountain, "Coronagraphic detection of Earth-like planets with large, actively controlled space telescopes," J. Astron. Telesc. Instrum. Syst. 8(4) 049002 (25 October 2022) https://doi.org/10.1117/1.JATIS.8.4.049002
4. Harvey, James & Kotha, Anita. (1995). Scattering effects from residual optical fabrication errors. Proceedings of SPIE - The International Society for Optical Engineering. 155-174. 10.1117/12.215588.
5. Stover, John C, Optical Scattering Measurement and Analysis, Third Edition, SPIE Press, 2012
6. James E. Harvey, Narak Choi, Andrey Krywonos, Gary L. Peterson, Marilyn E. Bruner, "Image degradation due to scattering effects in two-mirror telescopes," Opt. Eng. 49(6) 063202 (1 June 2010) https://doi.org/10.1117/1.3454382
7. Chris A. Mack, "Reducing roughness in extreme ultraviolet lithography," J. Micro/Nanolith. MEMS MOEMS 17(4) 041006 (7 August 2018) https://doi.org/10.1117/1.JMM.17.4.041006
8. Narak Choi, James E. Harvey, "Linear systems formulation of image analysis in the presence of both aberrations and surface scatter," Proc. SPIE 8128, Current Developments in Lens Design and Optical Engineering XII; and Advances in Thin Film Coatings VII, 81280B (7 September 2011); https://doi.org/10.1117/12.910930
9. William P. Zmek, Edward C. Moran, James E. Harvey, "The Effects Of Surface Quality Upon The Performance Of Normal Incidence X-Ray/XUV Imaging Systems," Proc. SPIE 0984, X-Ray Multilayers in Diffractometers, Monochromators, and Spectrometers, (16 December 1988); https://doi.org/10.1117/12.948788
10. J. M. Elson, H. E. Bennett, "Image Degradation Caused By Direct Scatter From Optical Components Into The Image Plane," Proc. SPIE 0511, Stray Radiation IV, (17 January 1985); doi: 10.1117/12.945028
11. Allen, Chris, "Surface Scattering", Course website URL people.eecs.ku.edu/~callen/823/EECS823.htm
12. Eugene L. Church and Peter Z. Takacs "Optimal estimation of finish parameters", Proc. SPIE 1530, Optical Scatter: Applications, Measurement, and Theory, (1 December 1991); https://doi.org/10.1117/12.50498
13. Nicodemus, F E, et al "Geometric Considerations and Nomenclature for Reflectance", US Dept of Commerce, Washington DC, NBS Monograph 160, 1977
14. Harvey, James E, Understanding Surface Scatter Phenomena a Linear Systems Formulation, SPIE Press, 2019
15. Hermansson, Forssell & Fagerstrom, "Review of Models for Scattering from Rough Surfaces", Swedish Defence Research Agency, ISSN 1650-1942, 2003.